Concentration of Vacancies at Metal-Oxide Surfaces: Case Study of MgO(100)

– Supplemental information –

N. A. Richter,[1] S. Sicolo,[2] S. V. Levchenko,[1] J. Sauer,[2] M. Scheffler[1]

[1]*Fritz-Haber-Institut der Max-Planck-Gesellschaft, Faradayweg 4-6, 14195 Berlin, Germany*
[2]*Institut für Chemie, Humboldt Universität zu Berlin, Unter den Linden 6, 10099 Berlin, Germany*

1 Calculations on embedded cluster models

Formation energies for F centers in MgO bulk, at the MgO(100) terrace, and at low coordinated sites were calculated with different methods, some of them using FHI-aims and TURBOMOLE to insure consistency of the two codes.

1.1 Cluster definition

Fig. S1 shows the cluster models that were employed for the DFT calculations of formation energies for defects at different configurational sites of the MgO(100) surface and in MgO bulk. All the clusters are embedded in a periodic array of point charges at the optimized PBE (pbc) cell parameter. For the surface models the positions of the point charges coincide with the coordinates of a relaxed defect-free 5-layer slab.

The CCSD(T) computations for the neutral oxygen vacancy in the bulk and at the MgO(100) terrace were performed using the embedded cluster models shown in Fig. S2. While all other embedded cluster calculations were performed with TURBOMOLE, this bulk model was also used for FHI-aims calculations at DFT level and for method validation employing G_0W_0@HSE.

1.2 Defect formation energies as a function of cluster size

To incorporate long-range polarization effects we extrapolate the DFT formation energies of the charged surface defects according to

$$G_f^q(n) = G_f^q(n \to \infty) + a\,(\frac{1}{n})^{\frac{1}{3}}, \tag{1.1}$$

where n is the number of ions in the cluster [1]. For all cluster calculations the Fermi level is at VBM and the chemical potential of oxygen is $\mu_{\mathrm{O}} = 1/2E_{\mathrm{O}_2}$. Since we do not relax all ions in the cluster, we use separate extrapolations for the vertical formation energy, $n = n_{\mathrm{total}}$, and for the relaxation energy, $n = n_{\mathrm{relax}}$. The formation energy of the relaxed defect is the sum of the vertical formation energy and the relaxation energy:

$$G_f^q = G_{f,\mathrm{vert}}^q + E_{\mathrm{relax}}^q. \tag{1.2}$$

With regard to the formation energies of the charged defects, we find that including long-range polarization effects is an important requirement for an accurate description, as mentioned by Sushko *et al*. [2]. The unrelaxed (vertical) formation energies and relaxation energies for F centers at MgO(100) have been obtained from a series of clusters including Mg_9O_9 (3×3×2 ions), $Mg_{25}O_{25}$ (5×5×2 ions) and $Mg_{50}O_{50}$ (5×5×4 ions). In Table S1 the vertical formation energies and relaxation energies obtained with PBE are summarized. The corresponding extrapolations are shown in Fig. S3.

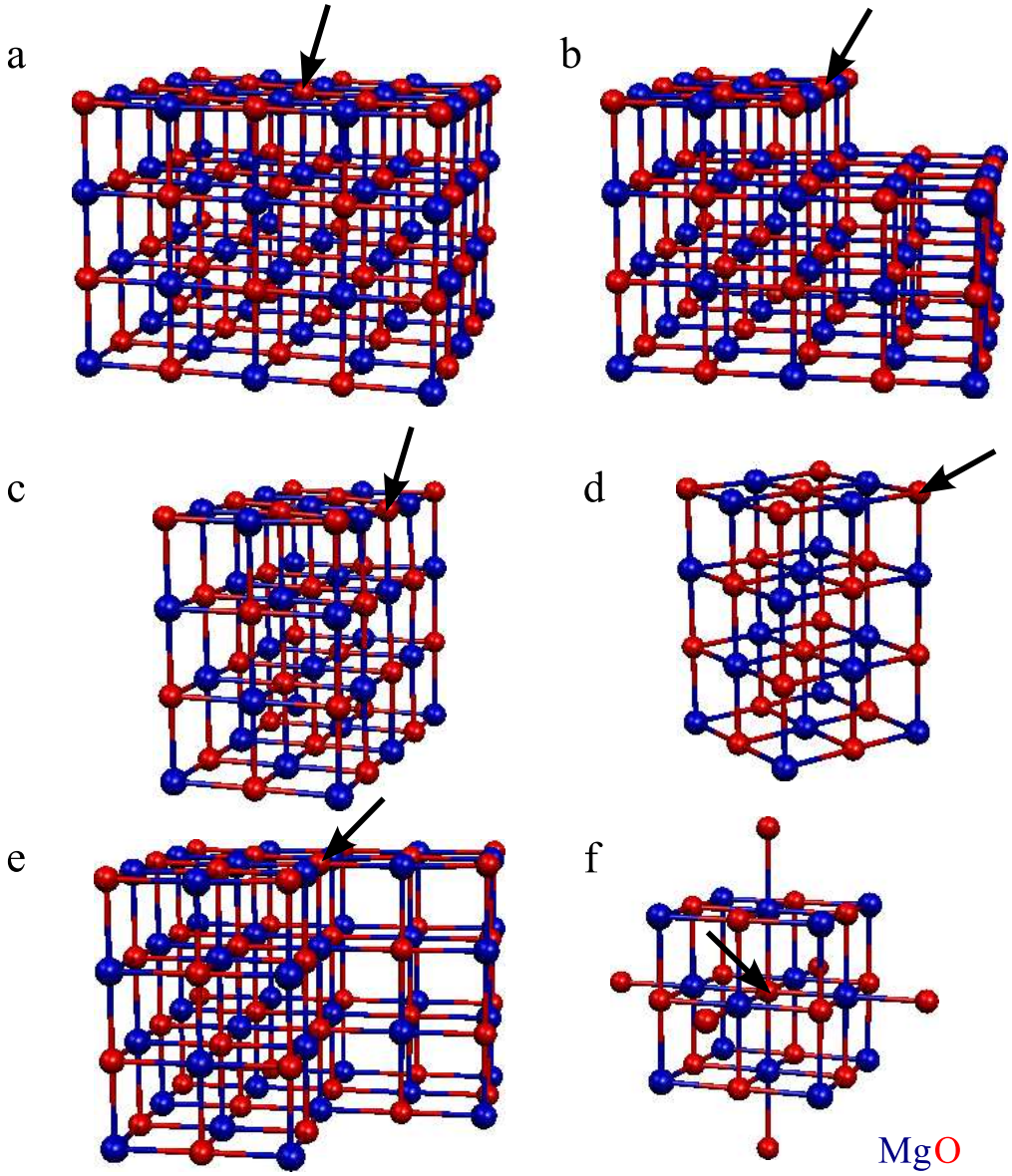

Figure S1: Cluster models for different sites: a) terrace ($Mg_{50}O_{50}$), b) step ($Mg_{45}O_{45}$), c) edge ($Mg_{30}O_{30}$), d) corner ($Mg_{18}O_{18}$), e) reverse corner ($Mg_{42}O_{42}$) and f) bulk ($Mg_{14}O_{19}$). The arrows indicate which atom was removed to form the defect.

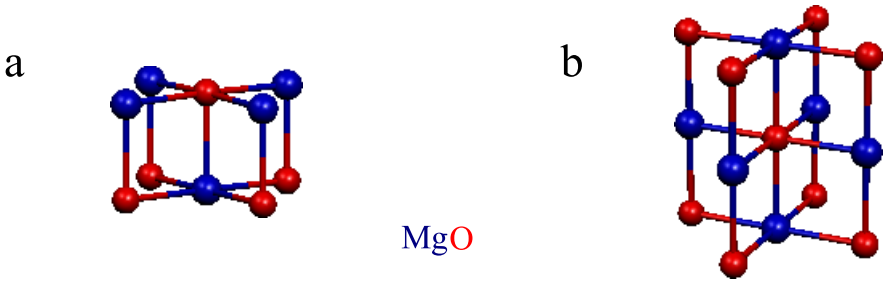

Figure S2: Cluster models for terrace (Mg_5O_5, a) and bulk (Mg_6O_9, b) used for comparison of DFT and CCSD(T) calculations.

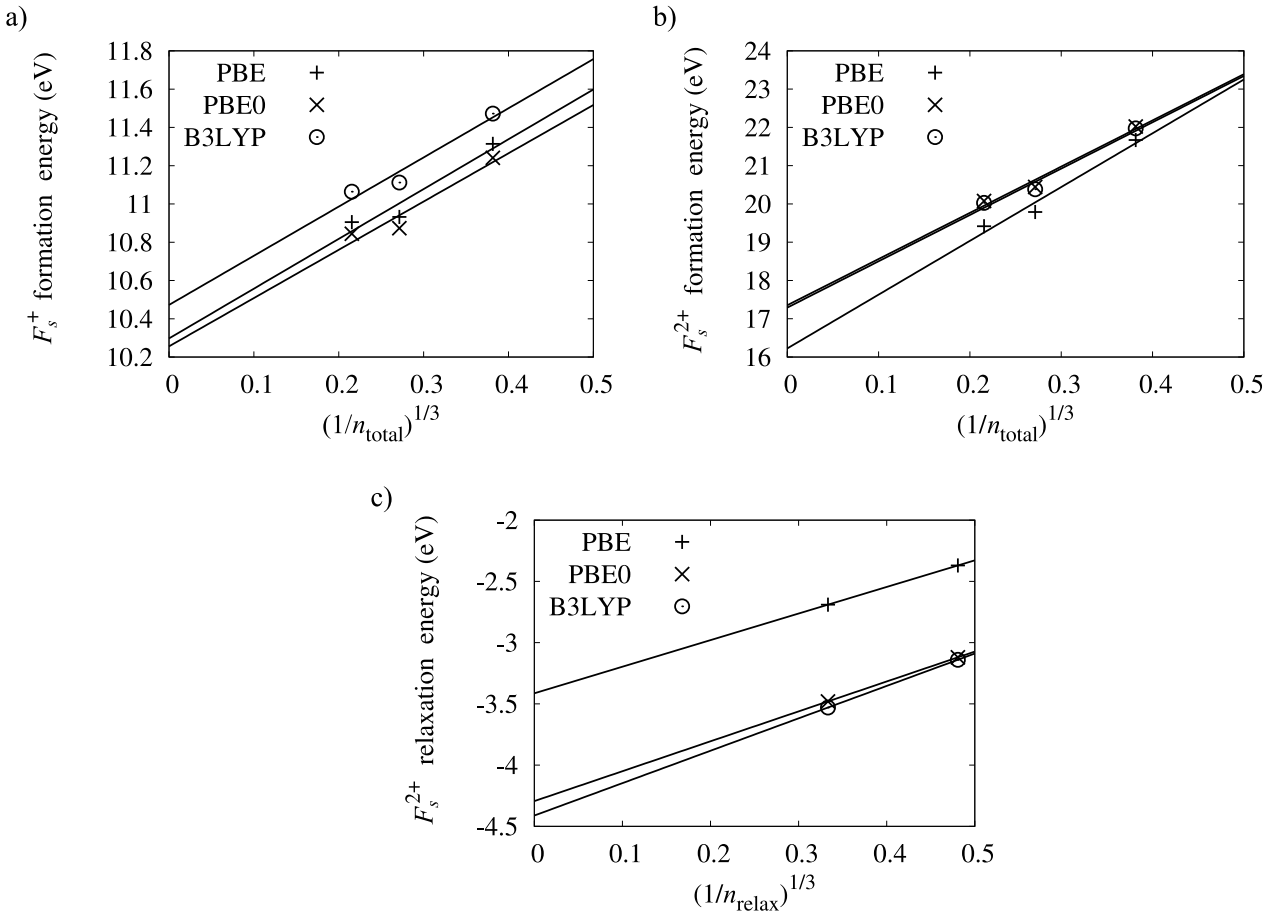

Figure S3: Extrapolated vertical formation energies for F_s^+ (a) and for F_s^{2+} (b), and extrapolated relaxation energy for F_s^{2+} (c), calculated with PBE, PBE0 and B3LYP.

Table S1: Vertical formation energies, relaxation energies, and formation energies including relaxation as obtained from embedded cluster and supercell calculations (PBE), all in eV.

Type of defect	Model	$G^q_{f,\text{vert}}$	E^q_{relax}	G^q_f
F_s^+	Supercell	10.71	-1.21	9.50
F_s^+	Emb. cluster	10.28	-0.81	9.47
F_s^{2+}	Supercell	16.54	-3.23	13.31
F_s^{2+}	Emb. cluster	16.21	-3.35	12.86

1.3 Comparison between DFT and CCSD(T) embedded cluster calculations for the neutral oxygen vacancy

Table S2 summarizes the vertical formation energies for a neutral F^0 center at the (100) terrace (Mg_5O_5) and in MgO bulk (Mg_6O_9). For consistency, bulk defect formation energies calculated with FHI-aims using a *tight*, tier 3 basis are shown, too. Also DFT formation energies using larger clusters are reported to show that the small clusters are already converged with respect to cluster size within 0.1 eV in vertical formation energy for the bulk defect and within 0.23 eV for the surface defect. In the main part of the paper we report the difference between the CCSD(T) and the DFT results, which can be used as a correction term to the DFT values.

Table S2: Vertical formation energies, G_f^q for F^0 and F_s^0 as obtained from embedded cluster DFT and CCSD(T) calculations, all in eV.

Defect site	Cluster model	PBE	PBE0	B3LYP	CCSD(T)
Terrace	Mg_5O_5	6.78	6.53	6.80	6.52
	$Mg_{50}O_{50}$	6.54			
Bulk	Mg_6O_9	7.18	7.02	7.37	7.09
	Mg_6O_9 (FHI-aims)	7.11	6.99	7.35	
	$Mg_{14}O_{19}$	7.06			

1.4 Obtaining the opt-HSE functional via ionization energies

Fig. 2 in the main paper shows ionization potentials $I^{q\to q+1}$ for $q = 0$ and $q = 1$ at F^0 geometry calculated for an Mg_6O_9 embedded cluster by ΔSCF with HSE xc functionals, and from the HOMO of a G_0W_0@HSE calculation (Eq. 3–4 in the main paper). The position of the "Fermi level" in these cluster calculations is defined as the ionization potential of the undefected cluster at bulk-like geometry. The results obtained with the ΔSCF method agree with the values obtained from the highest occupied Kohn-Sham levels at half occupation. Due to the small size of the cluster, the ionization potential $I^{+\to 2+}$ is shifted too far upwards with respect to $I^{0\to +}$. To remove the artificial overestimate, we shift to lower values the HSE and GW data for $q = 1$ by a constant (independent on α) value. This value is determined by averaging the difference between HOMO-1 (spin-minority channel) of the defected $(Mg_6O_{9-1})^+$ cluster, and HOMO-1 of the defected Mg_6O_{9-1} cluster. The position of the HOMO-1 orbital for each cluster represents the position of the Fermi level, and the difference between them is therefore an artifact of the cluster model. The resulting shift is -4.11 eV, and the uncertainty due to averaging is ± 0.1 eV. Note that this shift is not required to determine, and does not change, the optimal value of the parameter α, but is applied solely to give an estimate of the difference between $I^{0\to +}$ and $I^{+\to 2+}$ for the bulk based on the cluster models.

2 Extrapolation to dilute limit for periodic calculations

The formation energy of a neutral F center is already converged for a very small supercell of 64 atoms, while the formation energies of the F^+ and the F^{2+} centers show a strong dependence on L, the higher the charge state the more pronounced is the effect. The difference in formation energy for a 1728 atom supercell compared to a 1000 atom supercell is still 0.05 eV for the F^{2+} center. The leading contributions to the bulk defect formation energy dependence on the supercell size are the terms $\sim 1/L$ and $\sim 1/L^3$, where L is the supercell lattice constant. This implies that finite-size scaling according to

$$G_f^{\mathrm{bulk},q}(L,\epsilon_F,\mu_{\mathrm{O}}) = G_f^{\mathrm{bulk},q}(L\to\infty,\epsilon_F,\mu_{\mathrm{O}}) + \frac{a_1}{L} + \frac{a_2}{L^3} \tag{2.1}$$

leads to the correct formation energy in the dilute limit $G_f^{\mathrm{bulk},q}(L\to\infty)$.

The extrapolation procedure correctly incorporates the effects of atomic relaxation. Calculating supercells containing up to 2000 atoms for the doubly charged vacancies, using PBE exchange-correlation treatment, we get an accuracy of 0.05 eV for the extrapolated values of the formation energies. Vibrational contributions are estimated to be small and therefore neglected.

The defect formation energies calculated with HSE06 for the two smallest supercells (64 and 216 atom cells) lie exactly on the same fitting curve as the PBE formation energies, but shifted by a constant value (Fig. S4). Therefore, in all cases HSE formation energies are calculated for the smallest supercell, and then extrapolated to the dilute limit, where $1/L \to 0$, using a shifted PBE fitting function.

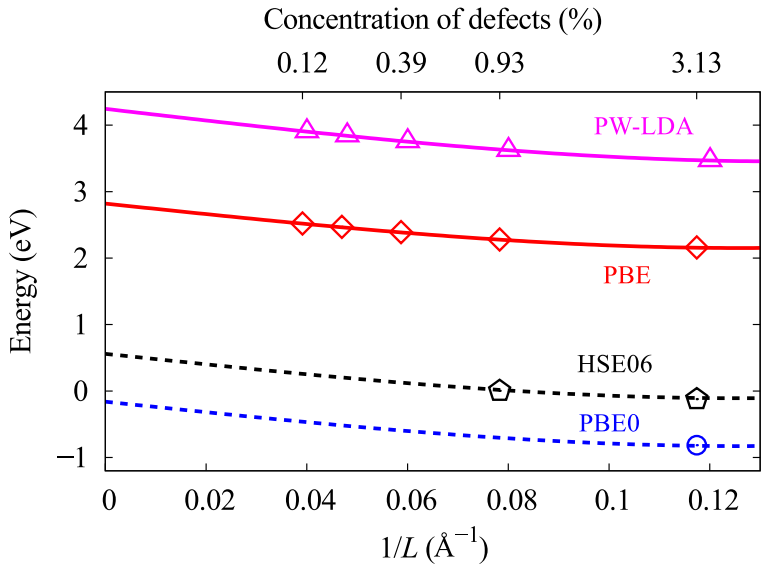

Figure S4: Finite-size scaling for the F^{2+} center formation energy (ϵ_F=VBM, $\mu_{\mathrm{O}} = 1/2\,E_{\mathrm{O}_2}^{\mathrm{tot}}$). Solid lines show fits to $\mathrm{G}_f^{\mathrm{bulk},2}(L) = a_0 + \frac{a_1}{L} + \frac{a_2}{L^3}$ for PW-LDA and PBE formation energies. Formation energies obtained with HSE06 lie on the shifted PBE curve. Accordingly, PBE coefficients a_1 and a_2 are used to extrapolate to isolated defects for all members of the HSE(α,ω) functional family.

Although computationally demanding, using the uniform neutralizing background method or the virtual crystal approximation together with extrapolation to the dilute limit is a reliable method for calculating formation energies of charged bulk defects. For charged surface defects, computed using VCA, the extrapolation is slightly different due to the broken symmetry at the surface. While for bulk supercells, the formation energies were fit to Eq. 2.1, where a term proportional to $\frac{1}{L^2}$ is zero due to symmetry reasons, for the surface

defects this term has to be included. The fitting function used is therefore

$$G_f^{\mathrm{VCA},q}(L,\epsilon_F,\mu_\mathrm{O}) = G_f^{\mathrm{VCA},q}(L\to\infty,\epsilon_F,\mu_\mathrm{O}) + \frac{a_1^q}{L} + \frac{a_2^q}{L^2} + \frac{a_3^q}{L^3}. \tag{2.2}$$

Two new aspects have to be taken care of when calculating the extrapolated formation energies for the isolated F centers at the surface. The periodicity of the calculation is three-dimensional, so the slabs are separated by vacuum to remove undesired interactions between repeating slabs. The reference unit cell is neutral, because the compensating charge $-q$ to the defect charge q is distributed on the Mg atoms in the slab. Since FHI-aims uses localized basis functions, there is no computational extra-cost when the vacuum region is chosen large. Here, the smallest distance between a defect and its image in z-direction, perpendicular to the surface, was chosen as 200 Å. Using a slab to model an isolated defect in a semi-infinite system only makes sense, if convergence of the desired property can be reached with respect to the number of layers N_L in the slab. The electrostatic energy in the slab depends obviously on N_L and this leads to different extrapolation curves, as shown for F_s^{2+} with slabs of N_L = 4,5,6, and 7 in Fig. S5. Full relaxation has been performed for all slab systems (using PBE), since also the geometric relaxation convergence and lattice polarizability may vary with N_L. While a 4 layer slab is not sufficient to obtain an accurate result for the extrapolated formation energy, where $1/L \to 0$, the 5 layer and 6 layer slab models yield the same value.

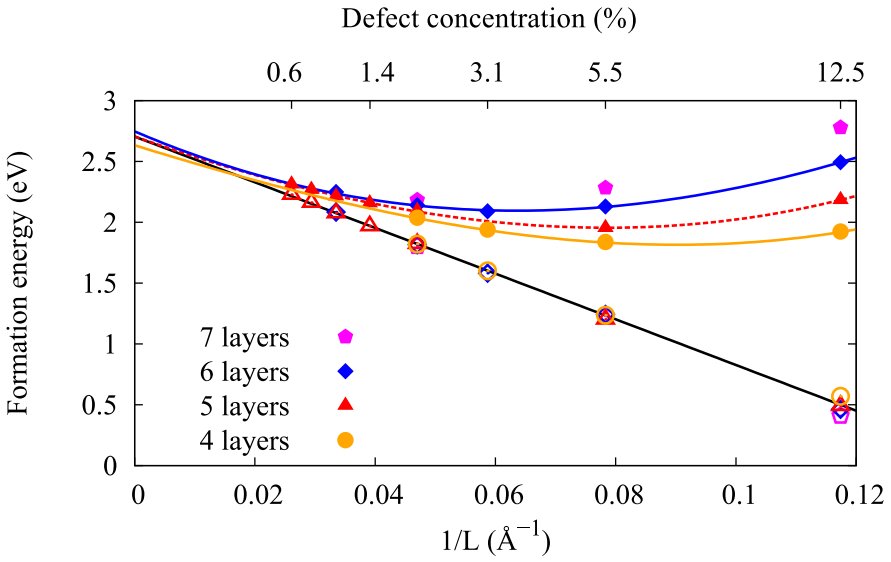

Figure S5: Extrapolation of the F_s^{2+} formation energy $G_f^{\mathrm{VCA},2}(L)$ (filled symbols, vibrations and dispersion neglected) to infinite supercell size ($L\to\infty$) for different numbers of layers in the slab, calculated with PBE. The Fermi level is at VBM and $\mu_\mathrm{O} = 1/2\,E_{\mathrm{O}_2}^{\mathrm{tot}}$. Open symbols and linear fit (black line) are obtained by subtracting the band bending contribution (Eq. 2.3).

The electrostatic energy that causes the formation energy of charged defects to increase with slab thickness d is the band bending (see main text). This contribution can be calculated as follows (see chapter 5 below):

$$qE^{\mathrm{SC}} = \frac{q^2 e}{6\epsilon_\mathrm{r}\epsilon_0}\frac{d}{L^2} \tag{2.3}$$

where e is the absolute value of electron charge. Subtracting qE^{SC} from the formation energies at every cell size $G_f^{\mathrm{VCA},q}(L)$ removes the term $\propto 1/L^2$ in the finite-size scaling curve for each slab thickness. This is shown on the example of the F_s^{2+} center ($q=2$) at the MgO(100) terrace in Fig. S5. The term $\propto 1/L^3$ plays a role only for small L, so that the remaining linear dependence coincides for slabs with a number of layers N_L = 4,5,6, and 7 for all calculated surface charge densities $\sigma = 2e/L^2$. The solid black line shows a linear fit, incorporating all calculated formation energies. This linear fit yields the same value for the formation energy of the isolated defect as obtained before for different slab thicknesses using Eq. 2.2. The linear term

is present due to the electrostatic attraction between the defects and the compensating charge. Thus, Eq. 2.2 yields full information on the dependence of the formation energy on defect concentration.

Eq. 2.2 can be generalized to the case when defects in different charge state (+ or 2+) coexist at the surface. First, we rewrite Eq. 2.2 in terms of surface charge density σ_q for $q = 1,2$ using $\sigma_q = qe/L^2$:

$$G_f^{\mathrm{VCA},q}(\sigma_q,d) = G_f^{\mathrm{VCA},q}(\sigma_q \to 0) + a_1^q \left(\frac{\sigma_q}{qe}\right)^{\frac{1}{2}} + a_2^q(d)\left(\frac{\sigma_q}{qe}\right) + a_3^q(d)\left(\frac{\sigma_q}{qe}\right)^{\frac{3}{2}}. \tag{2.4}$$

(Vibrational energy contributions to the formation energies are found to be insignificant for this study and therefore neglected.) When defects in both charge states are present at the surface simultaneously, the surface charge density is $\sigma = \sigma_1 + \sigma_2$. Since the nature of the second and third terms is purely electrostatic, we apply a mean-field approximation and simply replace σ_q with σ in these terms. The fourth term is more complicated since in addition to higher-order electrostatic effects it also includes geometric relaxation effects. However, also in this term we replace σ_q with σ, which corresponds to averaging the relaxation effects over different defect charge states. This averaging may give a noticeable error only in the specific case of comparable, and at the same time not small (> 3 %), concentrations of F_s^+ and F_s^{2+}. Thus, the dependence of the formation energies on the overall surface charge density σ is given by:

$$G_f^{\mathrm{VCA},q}(\sigma,d,\epsilon_F,\mu_{\mathrm{O}}) = G_f^{\mathrm{VCA},q}(\sigma \to 0,\epsilon_F,\mu_{\mathrm{O}}) + a_1^q \left(\frac{\sigma}{qe}\right)^{\frac{1}{2}} + a_2^q(d)\left(\frac{\sigma}{qe}\right) + a_3^q(d)\left(\frac{\sigma}{qe}\right)^{\frac{3}{2}}. \tag{2.5}$$

Note, that $G_f^{\mathrm{VCA},q}(\sigma \to 0)$ depends on Fermi energy ϵ_F and reservoir for oxygen atoms $\mu_{\mathrm{O}}(T,p_{\mathrm{O}_2})$. The calculated values of $G_f^{\mathrm{VCA},q}(\sigma \to 0)$ and a_i^q, $i =$ 1-3, for the 5-layer slab as obtained by extrapolation, are summarized in Table S3. The corresponding values, when a_2^q was extracted from Eq. 2.3 are shown in Table S4.

Table S3: $G_f^{\mathrm{VCA},q}(\sigma \rightarrow 0)$ as obtained with HSE06 and coefficients a_i^q, i = 1-3 for the 5-layer slab (ϵ_F=VBM, $\mu_{\mathrm{O}} = 1/2\, E_{\mathrm{O}_2}^{\mathrm{tot}}$)

q	$G_f^{\mathrm{VCA},q}(\sigma \rightarrow 0)(\mathrm{eV})$	$a_1^q(\mathrm{eV\AA})$	$a_2^q(\mathrm{eV\AA}^2)$	$a_3^q(\mathrm{eV\AA}^3)$
0	6.34	0	0	0
1	2.76	-4.93	24.76	42.29
2	0.55	-17.49	80.86	258.11

Table S4: $G_f^{\mathrm{VCA},q}(\sigma \rightarrow 0)$ as obtained with HSE06 and coefficients a_i^q, i = 1-3 for the 5-layer slab (ϵ_F=VBM, $\mu_{\mathrm{O}} = 1/2\, E_{\mathrm{O}_2}^{\mathrm{tot}}$), where a_2^q was obtained from Eq. 2.3

q	$G_f^{\mathrm{VCA},q}(\sigma \rightarrow 0)(\mathrm{eV})$	$a_1^q(\mathrm{eV\AA})$	$a_2^q(\mathrm{eV\AA}^2)$	$a_3^q(\mathrm{eV\AA}^3)$
0	6.34	0	0	0
1	2.77	-5.30	30.69	14.35
2	0.60	-20.13	122.78	62.93

3 Summary of formation energies for F centers in MgO in the dilute limit

Table S5: Formation energies $G_f^q(\sigma \rightarrow 0)$ (all in eV) of the F^0, F^+, and F^{2+} center in MgO bulk and the F_s^0, F_s^+, and F_s^{2+} center at the MgO(100) surface terrace site, calculated at different levels of exchange-correlation treatment within periodic boundary conditions (pbc) as well as using embedded cluster models (ecm). Periodic calculations and ecm computations with HSE06 have been performed with FHI-aims, while for all other ecm calculations TURBOMOLE was used. The Fermi level is at the VBM, where the VBM with respect to vacuum level was calculated using periodic slab models of the ideal surface. The chemical potential of oxygen is at the oxygen-rich limit where $\Delta\mu_{\mathrm{O}} = 0$. Our best numbers are highlighted in boldface.

Method	F^0	F^+	F^{2+}	F_s^0	F_s^+	F_s^{2+}
PBE-pbc	7.09	4.54	2.82	6.48	4.18	2.68
HSE06-pbc	**7.04**	**3.33**	**0.56**	**6.34**	**2.76**	**0.55**
PBE0-pbc	7.07	2.95	-0.16	6.33	2.56	0.12
HSE06-ecm	7.05	-	-	-	-	-
PBE-ecm[ΔCCSD(T)]	**6.94 [-0.09]**	-	-	**6.49 [-0.26]**	4.17	2.26
PBE0-ecm[ΔCCSD(T)]	**6.81 [+0.07]**	-	-	**6.26 [-0.01]**	2.54	-0.30
B3LYP-ecm[ΔCCSD(T)]	**7.17 [-0.28]**	-	-	**6.61 [-0.28]**	3.05	0.13

Table S6: Formation energies G_f^0 (all in eV) of the neutral F_s^0 center at the MgO(100) surface corner, reverse corner, step and edge, in the O-rich limit, calculated using embedded cluster models. For more information on these defects, see also Ref. [3].

Method	Reverse corner	Step	Edge	Corner
HF [4]	-	4.24	-	3.24
LDA [5]	6.76	6.99	-	5.45
PBE	5.94	5.68	5.76	5.13
PBE0	5.69	5.44	5.53	4.89
B3LYP [3]	5.91	5.61	5.78	5.01
B3LYP [2]	-	-	-	4.63

4 Valence-band maximum with respect to vacuum level

In the periodic calculations of the MgO(100) surface a vacuum region of ≈ 200Å separates repeating 5 layer MgO slabs. The potential in the middle of this vacuum region is the vacuum level $E^{\mathrm{Surf}}_{\mathrm{VAC}}$ for the surface calculation. To obtain the valence-band maximum (VBM) with respect to vacuum level for the bulk system, $E^{\mathrm{Bulk}}_{\mathrm{VBM-VAC}}$, a surface slab calculation is performed with the respective exchange-correlation functional and the difference between $E^{\mathrm{Surf}}_{\mathrm{VAC}}$ and the 1s core level of Mg in the deepest, bulk-like layer $E^{\mathrm{Surf}}_{\mathrm{core}}$ is determined. This difference is added to the Mg 1s core level in the bulk system $E^{\mathrm{Bulk}}_{\mathrm{core}}$ and the resulting bulk vacuum level is subtracted from the bulk VBM $E^{\mathrm{Bulk}}_{\mathrm{VBM}}$

$$E^{\mathrm{Bulk}}_{\mathrm{VBM-VAC}} = E^{\mathrm{Bulk}}_{\mathrm{VBM}} - \left(E^{\mathrm{Bulk}}_{\mathrm{core}} + (E^{\mathrm{Surf}}_{\mathrm{VAC}} - E^{\mathrm{Surf}}_{\mathrm{core}}) \right). \tag{4.1}$$

5 Concentration of surface defects

P-type dopants deep in the bulk set the Fermi level to VBM. As described in the main text, the formation energy of charged defects for a surface charge density σ is:

$$G_f^{\mathrm{VCA},q}(\sigma,z^{\mathrm{SC}}(\sigma)) = G_f^{\mathrm{VCA},q}(\sigma,d) - qE^{\mathrm{SC}}(\sigma,d) + qE^{\mathrm{SC}}(\sigma,z^{\mathrm{SC}}), \tag{5.1}$$

where $G_f^{\mathrm{VCA},q}(\sigma,d)$ is calculated by VCA and is given by Eq. 2.5, E^{SC} is the band bending contribution, and z^{SC} is the thickness of the space-charge layer. For a given concentration of dopants N_D,

$$z^{\mathrm{SC}} = \frac{\sigma}{eN_D}. \tag{5.2}$$

At temperature T = 0 K, the above z^{SC} minimizes the electrostatic energy of the system under the constraints of constant surface charge density and charge neutrality. At finite T, z^{SC} has a profile that minimizes the free energy of the system at that T. We estimated the effect of temperature on z^{SC}, and found it to be small at realistic T, σ, and N_D. Therefore, we use Eq. 5.2 to calculate z^{SC}. The formula for $E^{\mathrm{SC}}(\sigma,z^{\mathrm{SC}})$ is obtained by integrating the Maxwell equation for a charge density $\rho(\boldsymbol{r}) = \delta(z)\sigma - \sigma/z^{\mathrm{SC}}$:

$$\boldsymbol{E}_{\mathrm{z}} = \frac{\sigma}{\epsilon_r\epsilon_0}\left(1 - \frac{z}{z^{\mathrm{SC}}}\right)\boldsymbol{e}_{\mathrm{z}}, \tag{5.3}$$

where $\boldsymbol{E}_{\mathrm{z}}$ is the electric field along the surface normal $\boldsymbol{e}_{\mathrm{z}}$. $\sigma E^{\mathrm{SC}}(\sigma,z^{\mathrm{SC}})$ is the energy required to take electrons from the surface and distribute them uniformly over the thickness z^{SC}, recalculated per defect:

$$\sigma E^{\mathrm{SC}}(\sigma,z^{\mathrm{SC}}) = \frac{1}{2}\int_0^{z^{\mathrm{SC}}} E_z^2 dz = \sigma\frac{\sigma}{6\epsilon_{\mathrm{r}}\epsilon_0} z^{\mathrm{SC}}. \tag{5.4}$$

The potential difference $\Delta\phi$ due to band bending can be calculated by integrating Eq. 5.3:

$$\Delta\phi = -\frac{\sigma}{2\epsilon_r\epsilon_0} z^{\mathrm{SC}} \tag{5.5}$$

The change in Gibbs free energy per unit area upon defect formation is:

$$\Delta g(\eta_0,\eta_1,\eta_2,T,p_{\mathrm{O_2}},N_D) = \eta_0 G_f^0 + \sum_{q=1}^{2}\eta_q G_f^{\mathrm{VCA},q}(\sigma,z^{\mathrm{SC}}(\sigma,N_D)) - T\sum_{q=0}^{2} s^q_{\mathrm{conf}}(\eta_0,\eta_1,\eta_2), \tag{5.6}$$

where η_0, η_1, and η_2 are concentrations of the surface defects F_s^0, F_s^+, and F_s^{2+}, respectively, the total surface charge density $\sigma = e\eta_1 + 2e\eta_2$, and $s^q_{\rm conf}(\eta_0,\eta_1,\eta_2)$ is the configurational entropy per unit area. The configurational entropy accounts for all possible defect arrangements that have the same energy. Due to the screening of the charged defects by the compensating charge, the number of defect arrangements that have significantly different energy relative to the total number of possible arrangements at the surface for fixed η_0, η_1, and η_2 is expected to be small, and is vanishing for small defect concentrations. Equilibrium defect concentrations η_0, η_1, and η_2 can be found by minimizing Δg with respect to these concentrations:

$$\frac{\partial \Delta g}{\partial \eta_q} = G_f^q(\sigma,T,p_{\rm O_2},N_D,\epsilon_f) - T\frac{\partial \sum\limits_{r=0}^{2} s^r_{\rm conf}(\eta_0,\eta_1,\eta_2)}{\partial \eta_q} = 0. \tag{5.7}$$

Here, the formation energy

$$G_f^q(\sigma,T,p_{\rm O_2},N_D,\epsilon_F) = \frac{\partial}{\partial \eta_q}\sum_{r=0}^{2}\eta_r G_f^{{\rm VCA},r}(\sigma,T,p_{\rm O_2},N_D,\epsilon_F) \tag{5.8}$$

includes interaction between the defects. The configurational entropy for each type of defect is:

$$s^q_{\rm conf} = k_{\rm B}\left(\eta_q^{\rm sites}\ln\eta_q^{\rm sites} - \eta_q\ln\eta_q - (\eta_q^{\rm sites}-\eta_q)\ln(\eta_q^{\rm sites}-\eta_q)\right), \tag{5.9}$$

where $\eta_q^{\rm sites}$ is the surface density of available sites for the given type of defect:

$$\eta_q^{\rm sites} = \eta^{\rm sites} - \sum_{i\neq q}\eta_i. \tag{5.10}$$

For the MgO(100) surface, the surface density of oxygen atoms is $\eta^{\rm sites} = 0.11\cdot 10^{16}$ cm^{-2}.

For simplicity, we omit the derivation for equilibrium concentrations in the case when all defect charge states are present at the surface. Due to higher formation energies of F_s^0 and F_s^+ compared to F_s^{2+}, F_s^0 and F_s^+ concentrations are found to be relatively small, and can be omitted. The F_s^{2+} concentration, η_2, can then be found from the following equation:

$$G_f^2(2e\eta_2,T,p_{\rm O_2},N_D) - k_{\rm B}T\ln\frac{\eta^{\rm sites}-\eta_2}{\eta_2} = 0. \tag{5.11}$$

This equation can be easily solved numerically. The results are presented in the letter.

6 Molecular oxygen binding energy

It is well known that local and semi-local exchange-correlation functionals strongly overestimate the binding energy of O_2 [6, 7]. While in some cases it is beneficial to use the same approximation for all calculations related to a given problem since cancellation of errors is expected, this is often not the case for the O_2 binding energy. Indeed, we find that using the energy of the oxygen atom E_{O} as a reference, we obtain F^0 formation energies almost independent on the parameters of the HSE functional (see Table S7) and very close to the CCSD(T) corrected formation energies (see main paper), while at the same time the O_2 binding energy strongly depends on the HSE parameters (6.23 eV, 5.32 eV, and 5.38 eV for PBE, HSE06, and PBE0, respectively). Therefore, we use $\frac{1}{2}E_{\mathrm{O}_2}$ as a reference for the oxygen chemical potential, where $\frac{1}{2}E_{\mathrm{O}_2} = E_{\mathrm{O}} - \frac{1}{2}E_{\mathrm{O}_2}^{\mathrm{bind}}$, with the experimental binding energy without zero-point energies $E_{\mathrm{O}_2}^{\mathrm{bind}} = 5.22$ eV [8], and the total energy of the oxygen atom E_{O} calculated with the corresponding electronic structure approach.

Table S7: Formation energies for the neutral oxygen vacancy in MgO bulk (F^0, *left*) and the neutral oxygen vacancy at the MgO(100) surface (F_s^0, *right*) as obtained from supercell calculations for different values of the oxygen chemical potential μ_{O}, all in eV. (The basis settings used are the *tight* predefined settings.)

μ_{O}	PBE F^0	HSE06 F^0	PBE0 F^0	PBE F_s^0	HSE06 F_s^0	PBE0 F_s^0
E_{O}	9.70	9.65	9.68	9.09	8.95	8.94
E_{O_2}	6.59	6.99	6.99	5.98	6.29	6.25
$E_{\mathrm{O}} - \frac{1}{2}E_{\mathrm{O}_2}^{\mathrm{bind,exp}}$	7.09	7.04	7.07	6.48	6.34	6.33

Bibliography

[1] C. R. A. Catlow, I. D. Faux, and M. J. Norgett, J. Phys. C: Solid State Phys. **9**, 419 (1976)

[2] P. V. Sushko, A. L. Shluger, and C. A. Catlow, Surf. Sci. **450**, 153 (2000)

[3] S. Sicolo and J. Sauer, J. Phys. Chem. **117**, 8365 (2013)

[4] G. Pacchioni and P. Pescarmona, Surf. Sci. **412-413**, 657 (1998)

[5] L. Kantorovich, J. Holender, and M. Gillan, Surf. Sci. **343**, 221 (1995)

[6] M. Ernzerhof, J. P. Perdew, and K. Burke, Int. J. Quantum Chem. **64**, 285 (1997)

[7] J. P. Perdew, S. Kurth, A. Zupan, and P. Blaha, Phys. Rev. Lett. **82**, 2544 (1999)

[8] D. Feller and K. A. Peterson, J. Chem. Phys. **110**, 8384 (1999)